Calculation of Synthetic Energy Carrier Production Costs with high Temporal and Geographical Resolution

Uwe Langenmayr
Institute for Industrial Production
Karlsruhe Institute of Technology
Germany
uwe.langenmayr@kit.edu

Abstract

While the transition of the electricity sector proceeds, other sectors such as industry, transportation and agriculture may fall behind. One reason is the inability to electrify all processes. Power-to-X applications allow the transformation of these sectors by replacing conventional energy carriers with renewable synthetic energy carriers.

In this approach, the production costs of different synthetic energy carriers with a high temporal and spatial resolution are calculated. Hourly weather data of Australia and New Zealand with a spatial resolution of 0.25° x 0.25° are processed into capacity profiles. These capacity profiles, covering 11 years, are clustered into profiles including the representative weeks for each cell in the covered area using k-means clustering. The production processes of green hydrogen, ammonia, methanol and green crude are modeled with a generic linear program.

The results show that especially in Australia low production costs can be achieved. In combination with large land availability, this enables large-scale synthetic energy carrier production and possible export. Hydrogen derivatives are more expensive in production but transportation might play a significant role when deciding which synthetic energy carrier should be produced. Due to the spatial proximity to Australia, New Zealand might use this circumstance to import synthetic energy carriers in the early years and start domestic production when electrolysis achieves maturity.

Key words: Power-to-X, linear programming, k-means clustering, synthetic energy carriers

1 Introduction and Motivation

The mitigation of climate change is a major challenge of our society. The transformation of the electricity sector is in full swing using renewable generators like wind farms or photovoltaics. But the electricity sector is just the first step towards a climate neutral energy system. Other sectors such as industry, heating, agriculture and transportation sector need to increase their share of renewable energy as well. Especially the industry and agricultural sectors face the problem that electricity is only one form of required energy. Additionally, conventional energy carriers are used beyond solely energy provision.

Power-to-X (PtX) processes and technologies help to use renewable electricity beyond the direct replacement of conventionally generated electricity. With their application, several other forms of energy and synthetic energy carriers (SEC) can be generated or produced. Process

heating is one major energy consumer worldwide with a share of around 20% [16] of the global energy demand. Power-to-Heat applications allow especially low temperature heat supply. To cover the high temperature heat demand, PtX based energy carriers can be applied. Power-to-Gas applications allow the production of hydrogen (H_2) and synthetic natural gas. Synthetic natural gas can be used as energy carrier to provide high-temperature heat and closes the gap in the heat supply. But H_2 and synthetic natural gas further enable electricity generation via fuel cell or gas turbines. Furthermore, H_2 is used in several chemical processes like hydrocracking or hydrotreatment. In addition, H_2 allows the production of green steel via the direct reduction process. Power-to-Liquids and Power-to-Chem applications use synthesis to convert H_2 into other SECs. The production of green crude (GC) via Fischer-Tropsch (FT) processes allows the coverage of all conventional crude oil based products, allowing carbon neutral fuels for transportation, plastics, waxes and oils for the cosmetics industry. Green methanol (MeOH) produced via methanol synthesis (MeOH-Syn) can be used as solvent or in chemical processes, and its derivatives are used in pharmaceuticals. Finally, ammonia (NH_3) from the Haber Bosch (HB) synthesis is used to feed the world as it is the basis for fertilizer production. Altogether, PtX approaches help to replace conventional energy carriers without forgoing modern living standards.

Sets	
$c \in C$	Set of Conversion Components
$s \in S$	Set of Commodities
main input $\in MI$	Subset of S representing the Main Input of a Component
$s \in DS$	Subset of S representing the Demanded Commodities
$g \in G$	Set of Generators
$n \in N_c$	Set of Time Steps
Variables	
x_s	Quantity of Mass or Energy
$\mathrm{cap}_c, \mathrm{cap}_g, \mathrm{cap}_s$	Capacity of Component
$\mathrm{soc}_{s,t}$	State of Charge
i_c, i_g, i_s	Investment of Component
Parameters	
$P_{s,t}^{purchase}$	Purchase Price
$P_{s,t}^{sell}$	Selling Price
W_t	Weighting of Time Step t
D_s	Demand of Commodity s
$\mathrm{BU}_c^{upper}, \mathrm{BU}_c^{lower}$	Upper and Lower Bound of Capacity Utilization
$\mathrm{RAMP}_c^{up}, \mathrm{RAMP}_c^{down}$	Ramp-Up and Ramp-Down Rate
$\mathrm{CF}_{g,s,t}$	Capacity Factor
$\eta_{c,main\ in,s}^{out}$	Conversion Factor from MI to Output s
$\eta_{c,main\ in,s}^{in}$	Conversion Factor from MI to Input s
$\eta_s^{charge}, \eta_s^{discharge}$	Charging and Discharging Efficiency
$\mathrm{Inv}_c, \mathrm{Inv}_g, \mathrm{Inv}_s$	Investment of Components
$\mathrm{ANN}_c, \mathrm{ANN}_g, \mathrm{ANN}_s$	Annuity Factor of Component
$\mathrm{FOM}_c, \mathrm{FOM}_g, \mathrm{FOM}_s$	Fixed Operation and Maintenance
$\mathrm{VOM}_c, \mathrm{VOM}_g, \mathrm{VOM}_s$	Variable Operation and Maintenance
RPL	Representative Period Length
WACC	Weighted Average Cost of Capital

2 Literature Review, Research Questions & Structure

Techno-economic analysis of PtX processes have been conducted in process simulations, energy system models or stand-alone applications. This literature review focuses solely on

stand-alone applications including the integration of renewable energies via optimization methods as the review of all approaches is beyond the scope of this work, but [18] provides a broad view on other PtX research.

Recent publications increasingly use optimization models to integrate the volatile renewable generation. Linear programming models are applied to investigate the impact of volatile renewable generation on SEC production [21, 24, 27, 29]. [22] apply a mixed-integer linear program to model a superstructure with the aim to find the cost-minimal process path to produce syngas. Open source models have been implemented to either optimize the technical processes [2] or the electricity-based fuels production as a whole [19]. Larger scale production is optimized in [10] and [4] for the production of MeOH. [15] investigate the application of parallel methanol synthesis units regarding their ability to provide more flexibility. [30] use multi-objective optimization including efficiency and production costs to investigate the MeOH production.

The most similar approaches compared to our work are [9] and [26]. [9] use their baseload approach [7] which optimizes the production costs of H_2 while containing a steady H_2 supply. The H_2 production costs are used as input parameter for the following techno-economic analysis of the NH_3 production. The actual operation of the NH_3 synthesis is not considered and, therefore, it's flexibility unexploited. [26] apply their optimization model [25] in combination with weather data clustering to achieve high scalability of their model. Currently, this model is only applicable for NH_3 production as the model itself is not written generically.

In comparison to the above mentioned approaches, this approach implements a generic PtX model, which is applicable for several SECs. The model itself will be adjustable to different locations by integrating local data (e.g., weather data). Weather data clustering to obtain representative weeks for each cell in the considered grid is conducted. This allows scalability of the optimization to large areas. The main research questions of this approach are:

1. How can large-scale optimization approaches using spatial and temporal weather data with high resolution be conducted in appropriate time?
2. How can PtX approaches be modelled generically instead of the concentration on single SECs?
3. How does New Zealand and Australia perform regarding the production of SECs? What are the implications of the results?

The introduction, literature review and research questions in the chapter above are followed by the description of the applied methodology in Chapter 3. Chapter 4 presents the underlying data and PtX processes considered. The results are shown in Chapter 5, followed by a summary, conclusion and critical appraisal in the last chapter.

3 Methodology

In general, the approach is split into the processing of the weather data to obtain representative weeks of the renewable capacity factor profiles, and the optimization to minimize the production costs of the SECs. Figure 1 depicts the flow diagram of the process.

3.1 Deriving the Representative Capacity Factor Profiles

In the first step, the weather data features are processed to obtain the capacity profiles of different renewable generators. Here, the open source python application atlite [1] is applied and combined with technical data of different renewable generators to calculate their hourly

capacity profiles for each cell in the considered grid. This step is conducted using parallel processing to decrease the high computation time due to the high temporal and spatial resolution of the data.

The combination of a high spatial and temporal resolution within the data would result in large-scale optimization problems. To reduce the volume of data, k-means clustering is applied to derive representative weeks for each cell in the considered grid. Such an approach has the advantage that data is largely reduced but the information regarding utilization and volatility can be retained. The weekly capacity factor profiles of each generator is strung together to each other to create a vector (x_n). This is conducted for each week, creating the input matrix. A principal component analysis is used to reduce the dimension and choose the number of clusters based on the elbow method. The reduced matrix and the number of clusters are the input of the k-means clustering algorithm which has been applied in weather data clustering before [14, 20, 23] and provided suitable solutions, hence the application in this work. Equation (1) shows the mathematical description of k means [3].

$$\min_{b,\mu} J = \sum_{n}\sum_{k} b_{n,k} \|x_n - \mu_k\|^2 \quad (1)$$

The clustering will find K clusters with the cluster centers μ_k. Each vector x_n of the matrix N is assigned to one cluster. Which cluster the vector belongs to is decided via the binary variable $b_{n,k}$. The k-means clustering minimizes the total distance between each vector and the cluster center it belongs to by searching for the optimal location of the cluster center and the assignment of the vectors to the clusters. To obtain the representative weekly profile of a cluster, the vector, which is the closest to the cluster center, is chosen. The weights of the clusters are calculated by the number of weeks in the cluster divided by the total number of weeks in the matrix.

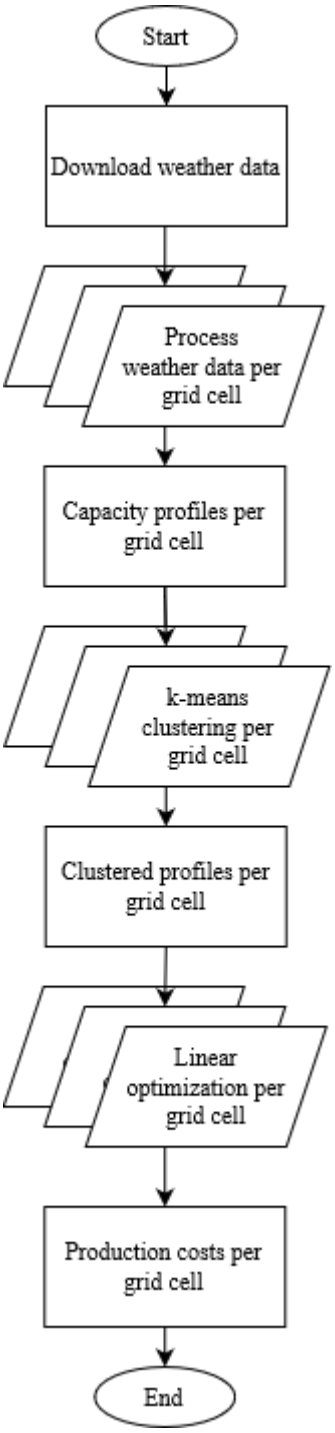

Figure 1: Flow diagram of the approach. Stacked boxed represent parallel processing

3.2 A Generic Linear Optimization Tool for PtX Processes

The following equations will describe the generic linear program to model a variety of PtX processes. The objective function includes the annualized initial investment and the maintenance of all conversion components, storage and generators.

$$\begin{aligned}\min f = &\sum_{c} i_c(\mathrm{ANN}_c + \mathrm{FOM}_c) + \sum_{s} i_s(\mathrm{ANN}_s + \mathrm{FOM}_s) \\ &+ \sum_{g} i_g\left(\mathrm{ANN}_g + \mathrm{FOM}_g\right) \\ &+ \sum_{t}\left(\sum_{s}\left(x_{s,t}^{charge}\cdot \mathrm{VOM}_s + \sum_{g} x_{g,s,t}^{generation}\cdot \mathrm{VOM}_g\right)\right. \\ &\left. + \sum_{c} x_{c,main\ in,t}^{in}\cdot \mathrm{VOM}_c\right)\cdot W_t\end{aligned} \tag{2}$$

3.2.1 Commodities

Commodities represent all mass and energy flows in the system and they connect all implemented components with each other. The detailed implementation of the commodities further allows an in-depth analysis of the results to understand the interaction between all elements of the system. The basic idea is the balancing of all commodities during all time steps, which is implemented in Equation (3).

$$\begin{aligned}&\sum_{c} x_{c,s,t}^{out} + x_{s,t}^{discharge} + \sum_{g} x_{g,s,t}^{generation} \\ &= \sum_{c} x_{c,s,t}^{in} + x_{s,t}^{charge} + x_{s,t}^{demand}\ \forall\ s,t\end{aligned} \tag{3}$$

The demand of a commodity forces the optimization to install certain capacities to provide the commodity. Equation (4) implements the yearly produced quantity of the commodity and enables a variable hourly production.

$$\sum_{t} x_{s,t}^{demand}\cdot W_t = D_s\ \forall\ s \in DS \tag{4}$$

3.2.2 Conversion Components

Conversion components enable the system to convert commodities and allows the system to produce the target product. Each conversion component consists of at least one conversion, but the implementation of several inputs and outputs is possible as well. Following equation defines the investment of each conversion component.

$$i_c = \mathrm{cap}_c \cdot \mathrm{Inv}_c\ \forall\ c \tag{5}$$

As mentioned above, each conversion component has at least one conversion, and, therefore, at least one input and one output. One input functions as connection between conversions and capacity. It is referenced as main input $x_{c,main\ in,t}^{in}$. Equation (6) defines the ratio between the main input and all outputs of the same conversion component. Equation (7) uses the same approach to define the ratio between the main input and all other inputs. The parameters $\eta_{c,main\ in,s}^{out}$ and $\eta_{c,main\ in,s}^{in}$ equal zero if commodities are not output nor input of the conversion component. To connect the main input and the capacity of the conversion component, Equation (8) is implemented. Equations (9) and (10) define the lower and upper bounds of the capacity utilization and the ramping ability of the conversion component.

$$x_{c,s,t}^{out} = x_{c,main\ in,t}^{in} \cdot \eta_{c,main\ in,s}^{out} \ \forall\ c, main\ in, s, t \tag{6}$$

$$x_{c,s,t}^{in} = x_{c,main\ in,t}^{in} \cdot \eta_{c,main\ in,s}^{in} \ \forall\ c, main\ in, s, t \tag{7}$$

$$x_{c,main\ in,t}^{in} \leq \mathrm{cap}_c \ \forall\ c, main\ in, t \tag{8}$$

$$\mathrm{cap}_c \cdot \mathrm{BU}_c^{lower} \leq x_{c,main\ in,t}^{in} \leq \mathrm{cap}_c \cdot \mathrm{BU}_c^{upper} \ \forall\ c, t \tag{9}$$

$$\mathrm{cap}_c \cdot \mathrm{RAMP}_c^{down} \leq x_{c,main\ in,t}^{in} - x_{c,main\ in,t-1}^{in} \leq \mathrm{cap}_c \cdot \mathrm{RAMP}_c^{up} \ \forall\ c, t \tag{10}$$

3.2.3 Renewable Generation Units

The following equation implements the possible hourly generation, which is dependent on the hourly capacity factor of the renewable energy and the capacity of the generator. Based on the capacity, the investment of the generator is calculated. If a commodity is not generated by a generation unit, the capacity factor equals 0 for all time steps.

$$x_{g,s,t}^{generation} \leq \mathrm{cap}_g \cdot \mathrm{CF}_{g,s,t} \ \forall\ g, s, t \tag{11}$$

$$i_g = \mathrm{cap}_g \cdot \mathrm{Inv}_g \ \forall\ g \tag{12}$$

3.2.4 Storage Components

The first storage constraint defines the storage activities and their impact on the hourly state of charge (SOC). To avoid that the storage is only depleted over the considered period, the last SOC of the representative period including the last storage activities have to be equal to the first SOC of the same representative period. Representative periods are connected via Equation (15). The SOC of the last hour of the previous representative period is defined by the storage activities of the last hour and the capacity of the storage component. This allows the disconnection of the SOC of the first hour of the following representative period from the storage activities of the previous representative period. Some storages are operated within a certain limit of the SOC (e.g., batteries to avoid degeneration). These limitations are imposed with Equation (16). Equations (17) and (18) define the ratio between charging and discharging activities, and the capacity of the storage component. The last equation defines the investment of the storage component.

$$\mathrm{soc}_{s,t} = \mathrm{soc}_{s,t-1} + x_{s,t-1}^{charge} \cdot \eta_s^{charge} - \frac{x_{s,t-1}^{discharge}}{\eta_s^{discharge}} \ \forall\ s, t \bmod \mathrm{RPL} \neq 0 \tag{13}$$

$$\mathrm{soc}_{s,t-RPL} = \mathrm{soc}_{s,t-1} + x_{s,t-1}^{charge} \cdot \eta_s^{charge} - \frac{x_{s,t-1}^{discharge}}{\eta_s^{discharge}} \forall\ s, t \bmod \mathrm{RPL} = 0 \tag{14}$$

$$\begin{aligned} \frac{x_{s,t-1}^{discharge}}{\eta_s^{discharge}} + \mathrm{cap}_s \cdot \mathrm{BU}_s^{lower} &\leq \mathrm{soc}_{s,t-1} \\ &\leq \mathrm{cap}_s \cdot \mathrm{BU}_s^{upper} - x_{s,t-1}^{charge} \cdot \eta_s^{charge} \ \forall\ s, t \bmod \mathrm{RPL} = 0 \end{aligned} \tag{15}$$

$$\mathrm{cap}_s \cdot \mathrm{BU}_s^{lower} \leq \mathrm{soc}_{s,t} \leq \mathrm{cap}_s \cdot \mathrm{BU}_s^{upper} \ \forall\ s, t \tag{16}$$

$$x_{s,t}^{charge} \leq \mathrm{cap}_s \cdot \mathrm{R}_s \ \forall\ s, t \tag{17}$$

$$x_{s,t}^{discharge} \leq \mathrm{cap}_s \cdot \mathrm{R}_s \ \forall\ s, t \tag{18}$$

$$i_s = \mathrm{cap}_s \cdot \mathrm{Inv}_s \ \forall\ s \tag{19}$$

4 Data

4.1 Weather data

This approach will cover the production of different SECs in Australia and New Zealand. The weather data of the two countries are processed with help from the open source tool atlite [1] using the techno-economic data in [6]. The tool calculates the hourly capacity profiles using the ERA 5 [13] data set which covers the whole globe and divides it into a grid with cell size 0.25° x 0.25°. Overall, the data covers an area of 7,956,021 km² and consists of 11,723 individual cells. Weather data years from 2010 to 2020 are considered to include the yearly variation of the weather. The yearly availability can vary significantly, and therefore needs to be considered when planning PtX facilities.

Table 1: Techno-economic data of renewable generators [6]

	2030		**2050**	
Technology	Wind	Solar	Wind	Solar
Turbine	Siemens Gamesa SG 5.0-145	-	Vestas V162-6.0 MW EnVentus	-
Rotor Diameter [m]	145	-	162	-
Hub Height [m]	100	-	110	-
Specific Power [W/m²]	303	-	291	-
Efficiency [%]	-	21.5	-	23
Nominal investment [€/kW]	1040	310	960	230
Fixed O&M [%]	1.21	1	1.18	1
Variable O&M [€/kWh]	0.00135	0	0.00122	0
Lifetime [years]	30	20	30	20

4.2 Considered Power-to-X Processes

To cover a broad spectrum of SECs, the production of H_2 and its processing to MeOH, GC and NH_3 is investigated. Figure 2 shows the production scheme of all SECs. The proton exchange membrane electrolysis (PEM) (3) has the advantage that it is able to react immediately on the volatile electricity generation. If the final product is MEoH, GC or NH_3, the H_2 is processed further. Here, CO_2 and nitrogen (N_2) are used as additional resources. Low-temperature air separation units (ASU) (5) are able to provide CO_2 and N_2 from ambient air, allowing the production of all SECs independent from point sources. In the case of NH_3, a Haber-Bosch synthesis is implemented to convert the H_2 and N_2 into NH_3. The GC route is implemented with a reverse water gas shift (rWGS) reactor, which converts the CO_2 and H_2 into synthetic gas. The synthetic gas is further processed in the FT synthesis to GC. The rWGS is assumed to be part of the synthesis for simplification. The methanol synthesis uses CO_2 directly in combination with H_2 to produce MeOH. All processes include H_2 (4) and battery storage (2). The processes are implemented with techno-economic data of the years 2030 and 2050 (Table 2, Table 3 and Table 4).

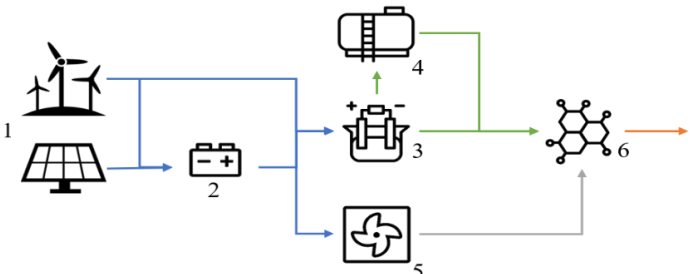

Figure 2. Structure of the SNC production process.

Table 2: Techno-economic data of PtX components

	PEM	CO_2 ASU	N_2 ASU	FT	MeOH-Syn	HB
Investment 2030	810 [€/kW]	1656 [€/kg/h]	224 [€/kg/h]	251 [€/kW]	235 [€/kW]	574 [€/kW]
Investment 2050	510 [€/kW]	736 [€/kg/h]				
Lifetime [years]	20	20	30	25	20	30
Fixed OM [%]	3.5	4	2	6	6	2
Min. Power [%]	0	0	0	80	40	30
Max. Power [%]	100	100	100	100	100	100
Ramp-Up [%/h]	100	100	100	20	20	20
Ramp-Down [%/h]	100	100	100	20	20	20
Reference	[12]	[8]	[17]	[12]	[28]	[17]

5 Results

The maps below show the H_2 production costs in New Zealand (NZ) and Australia (AU) for the years 2030 and 2050. The maps show clearly that the production costs in New Zealand are higher than in Australia. In NZ, especially the southern coastal regions of both islands perform the best, while this is the case in western AU. In addition, low production costs are possible in large areas of AU, resulting in the possibility of large-scale H_2 production and export. This creates the opportunity for New Zealand to import SECs from AU as long as the electrolysis technology is still premature and a domestic production unprofitable. In 2050, the production costs reduce due to the maturity of the electrolysis and ASU technologies. This allows cheaper domestic production in NZ as well.

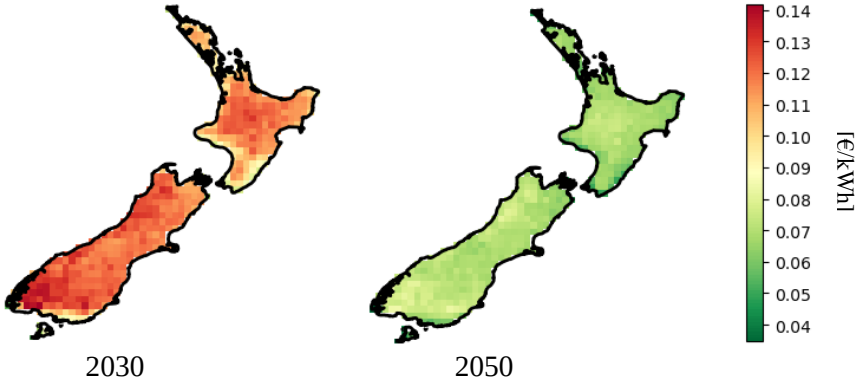

Figure 3: Production costs of H_2 in NZ

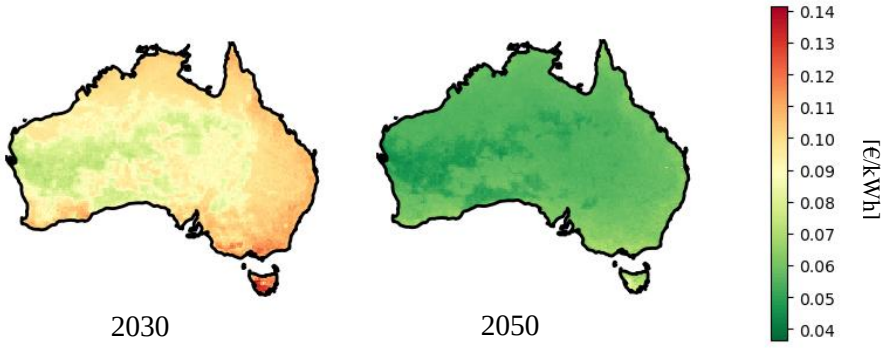

Figure 4: Production costs of H_2 in AU

The boxplots in Figure 5 show the distribution of production costs of H_2, MeOH, GC and NH_3. It is visible that H_2 is the cheapest option of all SECs. Other SECs need additional synthesis which not only increases the investment due to the additional equipment needed, but the H_2 needs to be supplied more steadily resulting in higher H_2 production costs due to additional storage capacities. The GC production, due to the lower flexibility, has the highest production costs, but the results show that the GC production can compete with the production of MeOH and NH_3 if the optimal location is chosen.

Table 3: Techno-economic parameters of storages

Parameter	**Battery**	**H_2 Storage**
Investment 2030 [€/kW]	200	15
Investment 2050 [€/kW]	150	
Lifetime [y]	15	20
Maintenance [%]	5	1
Charging Efficiency [%]	100	100
Discharging Efficiency [%]	92	100
Minimal SOC [%]	10	5
Maximal SOC [%]	90	100
Reference	[5]	[27]

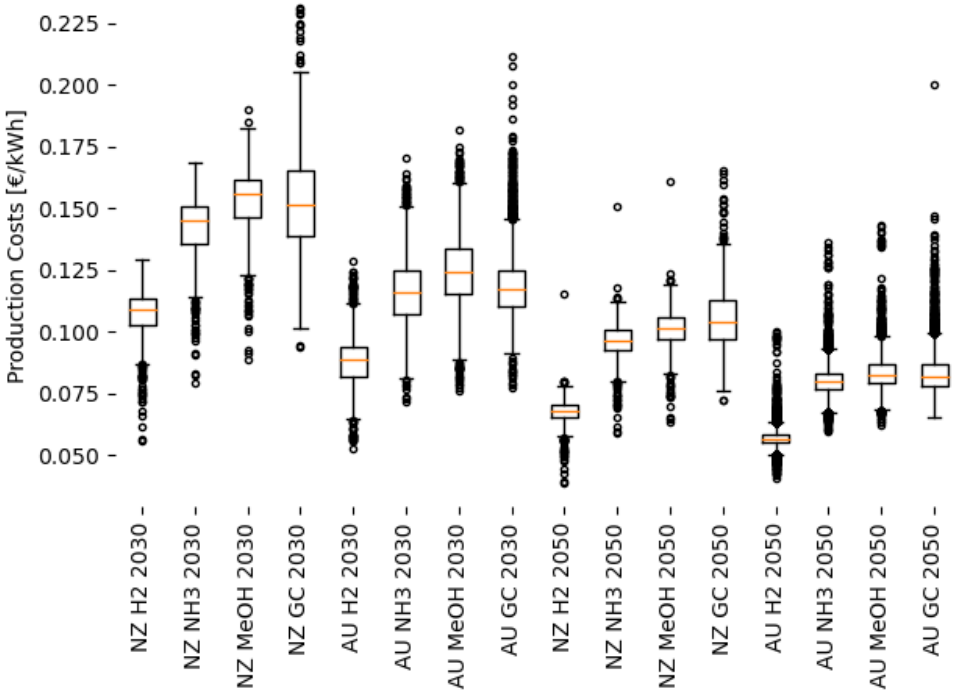

Figure 5: Production costs of different SECs at different locations and in different years

The production costs are only one factor in the supply chain of each SEC. The transportability of the SEC is a critical aspect, especially regarding long distance transportation. While H_2 has the lowest production costs, its energy density is low in comparison to other SECs and further steps (compression or liquification) need to be conducted before an economically feasible transportation is possible. Therefore, MeOH, NH_3 and GC might be more suitable if the SEC will be exported. Additionally, these SECs might be needed as chemical materials, making the synthesis indispensable

5.1 Computational Expenses

Within this approach, 187.8 GB of weather data has been downloaded and processed to 257,906 capacity profiles, each covering a whole year with an hourly resolution. These profiles have

been clustered into 23,446 profiles, each providing the representative weeks for one cell in the grid. The optimization model was implemented with the Python package Pyomo and solved with the commercial solver Gurobi [11]. Using parallel processing, the 93,784 linear optimizations took 5 days, 13 hours and 3 minutes. On average, setting-up, solving and processing the results of one optimization took 9 minutes and 47 seconds. All calculations have been performed on an AMD® Ryzen threadripper 3990x 64-core processor with 128 threads.

6 Summary, Conclusion & Future Work

This paper proposes a large-scale approach to calculate the production costs of green hydrogen, methanol, green crude and ammonia. The weather data of Australia and New Zealand of 11 years have been clustered to representative weeks. These representative weeks together with techno-economic data are the input of a generic linear optimization program to optimize the production costs. The results show that the production of synthetic energy carriers in Australia performs better. Furthermore, large areas of Australia have low production costs, resulting in potential large-scale synthetic energy carrier production.

For the sake of computability, this approach falls back on clustering of the data set. However, with such approaches, information in the data will always get lost and representative periods do not have the ability to represent the weather conditions perfectly. Therefore, the result cannot deliver exact data on local production costs. An investigation should be conducted to analyze the error resulting from this application and detailed analysis of the specific locations needs to be carried out if investments are realized. Furthermore, a simple linear program might not be sufficient to represent the real production conditions and is only an approximation. In addition, the production of SEC has not been implemented on a large scale. Therefore, current research still depends on assumptions and simplifications, as data is sparse.

The results deliver the production costs of SECs on a high spatial resolution. Production quantities, based on land availability data, can be combined with the production costs to create supply curves of SEC markets. The results include optimal capacities of all components, and the dispatch of auxiliary and operating materials. Based on this data, a life-cycle assessment can be conducted to further assess the environmental impact of the SEC production. A following step is the calculation of transportation costs of each SEC. They vastly differ regarding their transportation expenses which might affect the final decision which SEC will be produced.

Table 4: Input commodities of the PtX components

	Commodity	**Value**	**Ref**
PEM	Electricity [kWh]	1.61 (2030)	[12]
	Electricity [kWh]	1.466 (2050)	
	Desalinated Water [kg]	0.27	
DAC	Electricity [kWh]	0.225 (2030)	[8]
	Electricity [kWh]	0.182 (2050)	
N_2 ASU	Electricity [kWh]	0.243	[17]
FT	Electricity [kWh]	0.069	[12]
	Hydrogen [kWh]	1.435	
	CO2 [kg]	0.249	
MeOH	Electricity [kWh]	0.101	[28]
	Hydrogen [kWh]	1.145	
	CO2 [kg]	0.25	
HB	Electricity [kWh]	0.084	[17]
	Hydrogen [kWh]	1.12	
	N2 [kg]	0.16	

7 References

[1] Gorm B. Andresen, Anders A. Søndergaard, and Martin Greiner. 2015. Validation of Danish wind time series from a new global renewable energy atlas for energy system analysis. *Energy* 93, 612, 1074–1088. DOI: https://doi.org/10.1016/j.energy.2015.09.071.

[2] Mathias Berger, David Radu, Ghislain Detienne, Thierry Deschuyteneer, Aurore Richel, and Damien Ernst. 2021. Remote Renewable Hubs for Carbon-Neutral Synthetic Fuel Production. *Front. Energy Res.* 9. DOI: https://doi.org/10.3389/fenrg.2021.671279.

[3] Christopher M. Bishop. 2006. *Pattern recognition and machine learning*. Information Science and Statistics. Springer Science+Business Media LLC, New York, NY.

[4] Chao Chen and Aidong Yang. 2021. Power-to-methanol: The role of process flexibility in the integration of variable renewable energy into chemical production. *Energy Conversion and Management* 228, 6496, 113673. DOI: https://doi.org/10.1016/j.enconman.2020.113673.

[5] Wesley Cole and Frazier, Will, Augustine, Chad. 2021. *Cost Projections for Utility-Scale Battery Storage: 2021 Update* NREL/TP-6A20-79236, Golden, CO.

[6] Energistyrelsen - Danish Energy Agency. 2022. *Technology Data*. *Generation of Electricity and District heating*.

[7] Mahdi Fasihi and Christian Breyer. 2020. Baseload electricity and hydrogen supply based on hybrid PV-wind power plants. *Journal of Cleaner Production* 243, 306, 118466. DOI: https://doi.org/10.1016/j.jclepro.2019.118466.

[8] Mahdi Fasihi, Olga Efimova, and Christian Breyer. 2019. Techno-economic assessment of CO2 direct air capture plants. *Journal of Cleaner Production* 224, 957–980. DOI: https://doi.org/10.1016/j.jclepro.2019.03.086.

[9] Mahdi Fasihi, Robert Weiss, Jouni Savolainen, and Christian Breyer. 2021. Global potential of green ammonia based on hybrid PV-wind power plants. *Applied Energy* 294, 4, 116170. DOI: https://doi.org/10.1016/j.apenergy.2020.116170.

[10] Yu Gu, Danfeng Wang, Qianqian Chen, and Zhiyong Tang. 2022. Techno-economic analysis of green methanol plant with optimal design of renewable hydrogen production: A case study in China. *International Journal of Hydrogen Energy* 47, 8, 5085–5100. DOI: https://doi.org/10.1016/j.ijhydene.2021.11.148.

[11] LLC. Gurobi Optimization. 2022. *Gurobi Optimizer Reference Manual*.

[12] Paul Heinzmann, Simon Glöser-Chahoud, Nicolaus Dahmen, Uwe Langenmayr, and Frank Schultmann. 2021. *Techno-ökonomische Bewertung der Produktion regenerativer synthetischer Kraftstoffe. DOI: https://doi.org/*10.5445/IR/1000140638.

[13] Hans Hersbach, Bill Bell, Paul Berrisford, Shoji Hirahara, András Horányi, Joaquín Muñoz-Sabater, Julien Nicolas, Carole Peubey, Raluca Radu, Dinand Schepers, Adrian Simmons, Cornel Soci, Saleh Abdalla, Xavier Abellan, Gianpaolo Balsamo, Peter Bechtold, Gionata Biavati, Jean Bidlot, Massimo Bonavita, Giovanna Chiara, Per Dahlgren, Dick Dee, Michail Diamantakis, Rossana Dragani, Johannes Flemming, Richard Forbes, Manuel Fuentes, Alan Geer, Leo Haimberger, Sean Healy, Robin J. Hogan, Elías Hólm, Marta Janisková, Sarah Keeley, Patrick Laloyaux, Philippe Lopez, Cristina Lupu, Gabor Radnoti, Patricia Rosnay, Iryna Rozum, Freja Vamborg, Sebastien Villaume, and Jean-Noël Thépaut. 2020. The ERA5 global reanalysis. *Q.J.R. Meteorol. Soc.* 146, 730, 1999–2049. DOI: https://doi.org/10.1002/qj.3803.

[14] Peter Hoffmann and K. H. Schlünzen. 2013. Weather Pattern Classification to Represent the Urban Heat Island in Present and Future Climate. *Journal of Applied Meteorology and Climatology* 52, 12, 2699–2714. DOI: https://doi.org/10.1175/JAMC-D-12-065.1.

[15] Renxing Huang, Lixia Kang, and Yongzhong Liu. 2022. Renewable synthetic methanol system design based on modular production lines. *Renewable and Sustainable Energy Reviews* 161, 9, 112379. DOI: https://doi.org/10.1016/j.rser.2022.112379.

[16] IEA. 2018. *Clean and efficient hat for Industry* (2018). Retrieved November 4, 2022 from https://www.iea.org/commentaries/clean-and-efficient-heat-for-industry.

[17] Jussi Ikäheimo, Juha Kiviluoma, Robert Weiss, and Hannele Holttinen. 2018. Power-to-ammonia in future North European 100 % renewable power and heat system. *International Journal of Hydrogen Energy* 43, 36, 17295–17308. DOI: https://doi.org/10.1016/j.ijhydene.2018.06.121.

[18] Alper C. Ince, C. O. Colpan, Anke Hagen, and Mustafa F. Serincan. 2021. Modeling and simulation of Power-to-X systems: A review. *Fuel* 304, 121354. DOI: https://doi.org/10.1016/j.fuel.2021.121354.

[19] Philipp Kenkel, Timo Wassermann, Celina Rose, and Edwin Zondervan. 2021. A generic superstructure modeling and optimization framework on the example of bi-criteria Power-to-Methanol process design. *Computers & Chemical Engineering* 150, 107327. DOI: https://doi.org/10.1016/j.compchemeng.2021.107327.

[20] John W. Kidson. 1994. Relationship of new zealand daily and monthly weather patterns to synoptic weather types. *Int. J. Climatol.* 14, 7, 723–737. DOI: https://doi.org/10.1002/joc.3370140703.

[21] Georg Liesche, Dominik Schack, and Kai Sundmacher. 2019. The FluxMax approach for simultaneous process synthesis and heat integration: Production of hydrogen cyanide. *AIChE J* 65, 7, e16554. DOI: https://doi.org/10.1002/aic.16554.

[22] Andrea Maggi, Marcus Wenzel, and Kai Sundmacher. 2020. Mixed-Integer Linear Programming (MILP) Approach for the Synthesis of Efficient Power-to-Syngas Processes. *Front. Energy Res.* 8. DOI: https://doi.org/10.3389/fenrg.2020.00161.

[23] Robert Neal, David Fereday, Ric Crocker, and Ruth E. Comer. 2016. A flexible approach to defining weather patterns and their application in weather forecasting over Europe. *Met. Apps* 23, 3, 389–400. DOI: https://doi.org/10.1002/met.1563.

[24] Ola Osman, Sgouris Sgouridis, and Andrei Sleptchenko. 2020. Scaling the production of renewable ammonia: A techno-economic optimization applied in regions with high insolation. *Journal of Cleaner Production* 271, 1, 121627. DOI: https://doi.org/10.1016/j.jclepro.2020.121627.

[25] Nicholas Salmon and René Bañares-Alcántara. 2021. Impact of grid connectivity on cost and location of green ammonia production: Australia as a case study. *Energy Environ. Sci.* 14, 12, 6655–6671. DOI: https://doi.org/10.1039/d1ee02582a.

[26] Nicholas Salmon and René Bañares-Alcántara. 2022. A global, spatially granular techno-economic analysis of offshore green ammonia production. *Journal of Cleaner Production* 367, 3, 133045. DOI: https://doi.org/10.1016/j.jclepro.2022.133045.

[27] Dominik Schack, Liisa Rihko-Struckmann, and Kai Sundmacher. 2016. Structure optimization of power-to-chemicals (P2C) networks by linear programming for the economic utilization of renewable surplus energy. In *26th European Symposium on Computer Aided Process Engineering*, Miloš Bogataj and Zdravko Kravanja, Eds. Computer Aided Chemical Engineering, volume 38. Elsevier, Amsterdam, Netherlands, 1551–1556. DOI: https://doi.org/10.1016/B978-0-444-63428-3.50263-0.

[28] Felix Schorn, Janos L. Breuer, Remzi C. Samsun, Thorsten Schnorbus, Benedikt Heuser, Ralf Peters, and Detlef Stolten. 2021. Methanol as a renewable energy carrier: An assessment of production and transportation costs for selected global locations. *Advances in Applied Energy* 3, 12, 100050. DOI: https://doi.org/10.1016/j.adapen.2021.100050.

[29] Evan D. Sherwin. 2021. Electrofuel Synthesis from Variable Renewable Electricity: An Optimization-Based Techno-Economic Analysis. *Environmental science & technology* 55, 11, 7583–7594. DOI: https://doi.org/10.1021/acs.est.0c07955.

[30] Hanfei Zhang, Ligang Wang, Jan van herle, François Maréchal, and Umberto Desideri. 2019. Techno-Economic Optimization of CO2-to-Methanol with Solid-Oxide Electrolyzer. *Energies* 12, 19, 3742. DOI: https://doi.org/10.3390/en12193742.